DOI:10.1190/segam2020-3419066.1

Influence of gauge length on DAS VSP data at the Houston Research Center Test Well

Ezzedeen Alfataierge, Ali Aldawood, and Andrey Bakulin, Saudi Aramco EXPEC Advanced Research Center; Robert R. Stewart, University of Houston; Harold Merry, Aramco Americas

Summary

A series of tests have been conducted at the Aramco Houston Research Center (HRC) fiber-optic test facility, assessing the influence of DAS gauge length (G_L) on VSP data. This study demonstrates this influence in a shallow (1,500 ft) test well equipped with geophones and fiber-optic cables cemented behind the casing. G_Ls of 2, 4.5, 9, and 12 m are investigated in comparison to vertical geophone data with approximately 11 m receiver spacing. The results show that the optimal G_L was 4.5 m, which corresponded to about one-quarter of the dominant seismic wavelength. The optimal G_L was obtained by investigating the signal-to-noise ratio of the field shot-records with respect to the various processing products, as well as, the cross-correlation of the DAS corridor-stacks with the geophone corridor-stack. Additionally, we show that the velocity profiles obtained using various G_Ls were comparable with minimal variation of ±20 m/s. In conclusion, we recommend selecting the G_L based on the expected average formation velocity and maximum seismic frequency in order to record optimal DAS VSP data.

Introduction

Distributed Acoustic Sensing (DAS) has shown promising results over the years (Meystayer et al., 2011; Mateeva et al., 2012) with critical evaluations on the limitations of fiber-optic sensing (Willis et al., 2016; Wu et al., 2017). The influence of gauge length (G_L) has been demonstrated on synthetic data by Dean et al. (2016), whereas Hardeman-Vooys and Lamoureux (2019) showed that an observed wavelet peak flattens as the G_L approaches the spatial wavelength of the wavelet, thus resulting in a doublet when the G_L is larger than the spatial wavelength. Therefore, it is essential to select the optimal G_L to avoid suppression of the primary signal energy by DAS array.

The fiber-optic test facility was established at the Aramco Houston Research Center, to evaluate various aspects of DAS acquisition technologies. The facility hosts a shallow test well, around 1,500 ft (~460 m) deep, equipped with multiple optical fiber cables and a string of vertical geophones cemented behind casing, as seen in Figure 1. In this paper, we present the results of a zero-offset VSP (11 m offset) survey conducted using a Vibroseis source with a 12s linear sweep from 8 to 120 Hz. We compare the geophone measurements to DAS recordings with cables cemented behind casing.

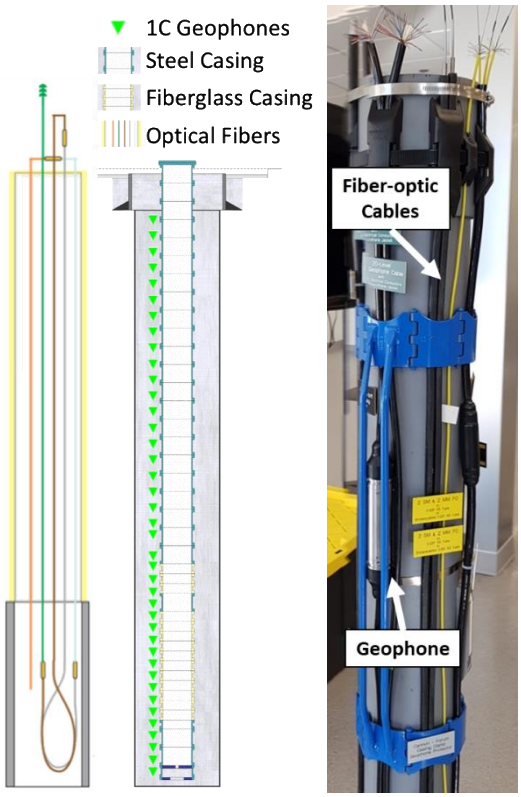

Figure 1: Schematic of fiber and geophone installation behind the casing (left) and actual size replica of the downhole setup with the geophone and fiber-optic cables clamped to casing (right).

Methodology

In a dual-pulse DAS interrogation system, the G_L can be defined as the distance between the two pulses and is calculated using the optical parameters of pulse-width (P_w) and pulse-gap (P_g), and the speed of light in the fiber (V) controlled by the speed of light in a vacuum (C) and the fiber refractive index (n)

$$G_L = V\left(\frac{P_w + P_g}{4}\right) \text{ where } V = \frac{C}{n} \quad (1)$$

Definitions and units of each quantity are as follows:

G_L: Gauge Length (m) V : Speed of Light in Fiber (m/s)
P_w: Pulse Width (ns) C : Speed of Light in Vacuum (m/s)
P_g : Pulse Gap (ns) n : Fiber Refractive Index (unitless)

The optical G_L parameters are presented in Table 1 along with the approximated G_Ls.

Table 1: DAS Gauge Lengths along with the optical recording parameters of pulse-width (P_w) and pulse-gap (P_g)

P_w (ns)	P_g (%)	G_L (m)
30	20	2
70	30	4.5
130	40	9
	80	12

Data Processing

Similar data processing was conducted on both geophone and DAS data. DAS data were analyzed as is, without any DAS to geophone conversion. DAS data required some additional pre-processing steps to suppress common-mode noise (CMN) and identify the exact position of well top and bottom. CMN is characterized by flat events in time. These events are constant along the fiber length but variable in time, as a result of ambient noise at the DAS interrogator being imprinted on the data.

The CMN was suppressed by applying a large median filter (~200 traces) on the data and subtracting the result from the initial dataset. Whereas, picking the well top and bottom was assisted by field measurements of a tap test on the well head to isolate the location of the well top on the record, and using the maximum first break pick as the well bottom. We found that, we were able to verify these measurements using the tube wave reflection points at the bottom and top of the well.

Next, the geometry is updated and first-breaks are picked similarly for geophone and DAS data. For wavefield separation and deconvolution the parameters were distinct for DAS and geophone data given the significant difference in spatial sampling (around 11 m for geophone and 0.67 m for DAS). Similarly, larger median filter windows were used during the wavefield separation of DAS data versus the geophone data. The final processing step consisted of amplitude correction for spherical divergence, FK-filtering, tube-wave suppression, bandpass filtering, and corridor muting, to generate the corridor stack.

Geophone data processing results are presented in Figure 2: the original correlated shot record (Figure 2a), the up-going separated wavefield (Figure 2b), and the final upgoing wavefield after special processing (Figure 2c). We note that the geophone data are spatially aliased due to the sparse geophone spacing and the relatively short seismic wavelength. Nevertheless, upgoing reflections are evident, but the records remain contaminated with downgoing and upgoing tube waves. Tube waves are suppressed during special processing in two steps. First, the downgoing tube waves are picked and separated via wavefield separation. Then, an FK filter is designed to suppress any remaining tube waves.

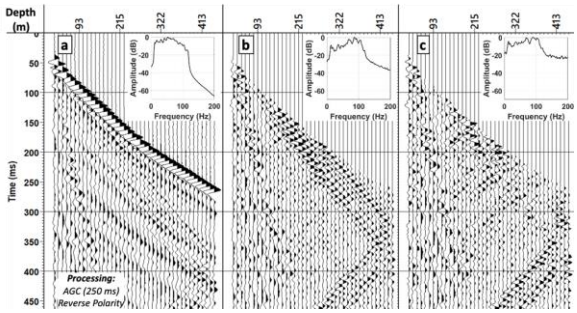

Figure 2: Geophone ZVSP processing results with a 250 ms AGC window applied, and the polarity reversed for visualization: (a) correlated shot record, (b) upgoing wavefield after wavefield separation and deconvolution, and (c) upgoing wavefield after special processing. The corresponding frequency spectrum for each record is shown in the top right.

Data Analysis

SNR Analysis

The signal-to-noise ratio (SNR) for each record is computed as the spectral amplitude ratio between a window before the first breaks (noise) and a window containing early arrivals (signal). Figure 3 shows an example of such computation by making a difference in the average amplitude spectra between two windows over the entire frequency range in dB scale: an average signal (pink rectangle) of -70 dB and an average noise (green rectangle) of -90 dB yields an SNR of 20.

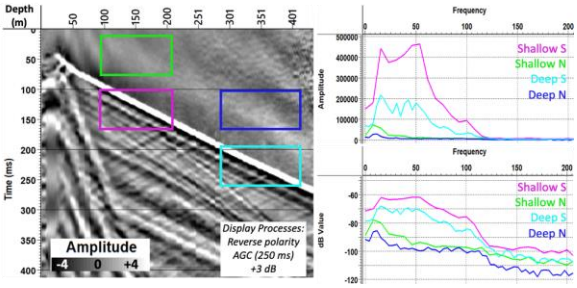

Figure 3: SNR is estimated as subtraction between the average amplitude level of the signal (early arrivals) and noise before the first breaks (pink and cyan rectangles).

The SNR estimates are used to compare the DAS records at various GLs quantitatively. We find SNR of 7, 25, 9, and 15 at the G_Ls of 2 m, 4.5 m, 9 m, and 12 m, respectively. The highest SNR is obtained at a G_L of 4.5 m that is also validated visually by the image showing sharper events that appear smeared at larger G_Ls (Figure 4a).

DOI:10.1190/segam2020-3419066.1

After processing the data to unveil the deconvolved up-going wavefield (Figure 4b), we find that the overall SNR reduces for all records. The largest G_L of 12 m now has the highest SNR of 15 versus the SNR of 10 for G_L of 4.5 m. However, the SNR does not capture the visual attribute of the sharpness of the up-going reflections.

Proceeding to corridor stacks (Figure 5), we find that the highest correlation between the DAS and geophone data (0.65) is achieved at 4.5 m G_L, providing additional support to select this G_L as optimal.

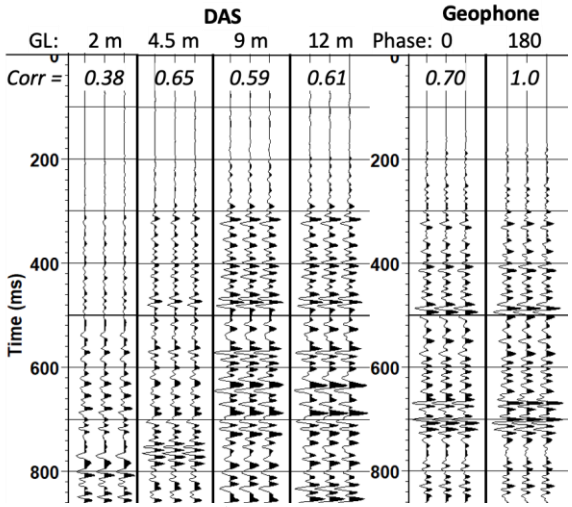

Figure 5: Correlation of DAS corridor-stacks with geophone corridor-stacks shown for different G_L.

Velocity Analysis

Using the first break picks (FBP) from each zero-offset VSP record, we can establish a relationship between seismic time and measured depth that is typically used to tie seismic images to well logs. Additionally, using the FBP, we can calculate the interval and RMS velocities along the wellbore.

The FBP of the geophone and DAS records are plotted in Figure 6a, where we see an overall match between DAS and geophone picks with minor variation in DAS picks with respect to change in G_L. We observe that DAS picks match geophone picks with reverse polarity in a shallower interval, whereas in a deeper section, they are closer to geophone picks with positive polarity.

Using the dense DAS FBP to compute the interval velocity results in large errors of interval properties, which results in incorrect RMS velocities. Decimating the FBP is one simple solution to produce more robust interval and RMS velocities. Figure 6b shows high deviations in interval velocities prior to FBP decimation and closer matching between geophone and DAS interval velocities after FBP decimation. Similarly, the RMS velocity is overestimated by approximately 200 m/s, which is resolved to produce similar geophone RMS velocities after FBP decimation. Another way to address this issue is to perform a regularized velocity inversion in a least-squares and accommodate small errors in picks (Lizarralde and Swift, 1999).

Conclusions

We demonstrate that DAS was able to produce comparable VSP measurements to geophones with both sensing instruments cemented behind the casing. Further analysis is required to quantify the amplitude fidelity of both systems. G_L makes a significant influence on DAS data that acts as an array filter analogous to the geophone groups in surface seismic. Optimal G_L is expected to maximize SNR while avoiding suppression of the desired signal. We observe that the decimation of DAS FBP helps to reduce the differences in velocity analysis results between geophone and DAS data. Fiber behind the casing enables the acquisition of high-quality DAS VSP data that enables flexible acquisition with various G_L and user-controlled receiver sampling.

10.1190/segam2020-3419066.1

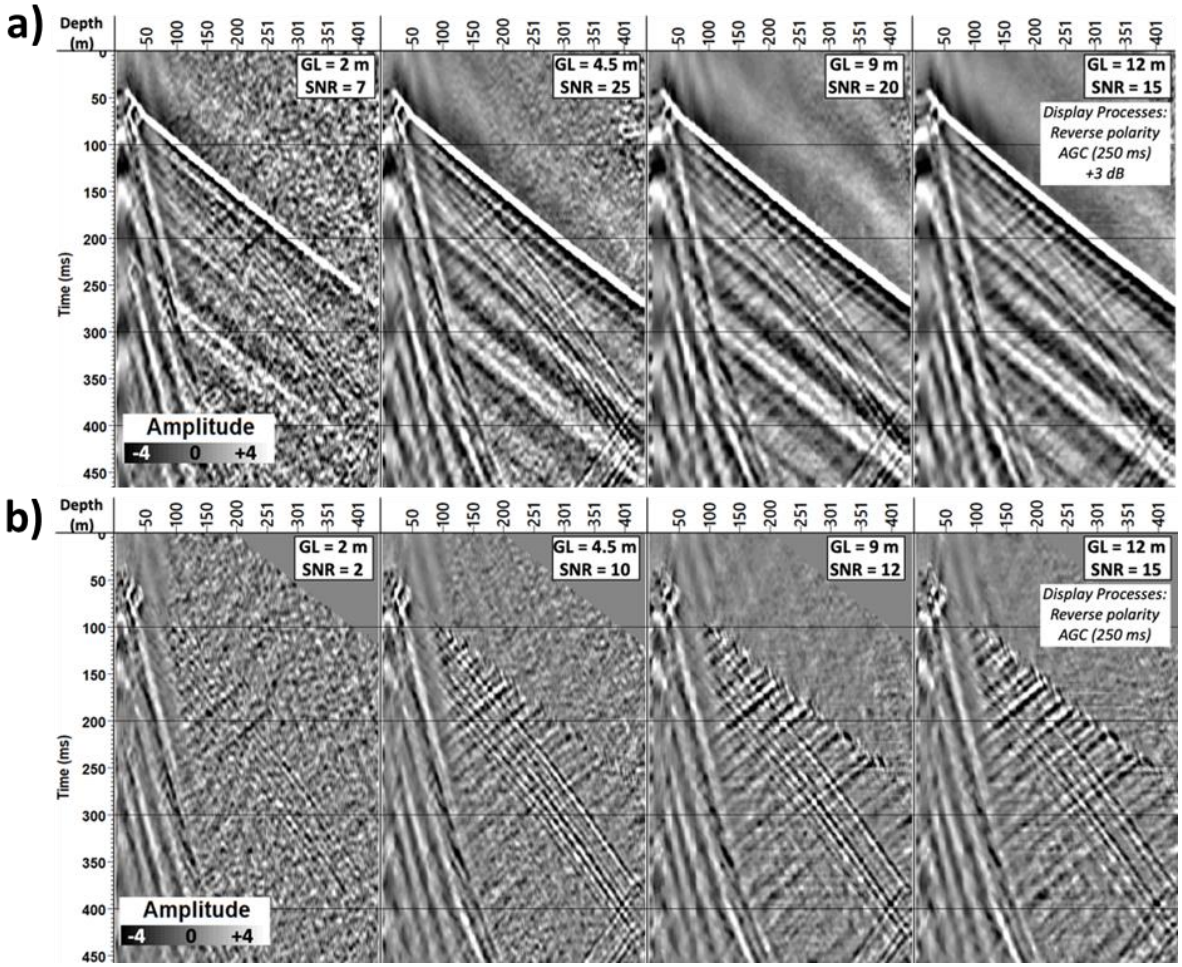

Figure 4: Results of DAS VSP processing: (a) DAS zero-offset VSP records after CMN suppression recorded with a different G_Ls; (b) same as (a) but showing upgoing wavefield after deconvolution.

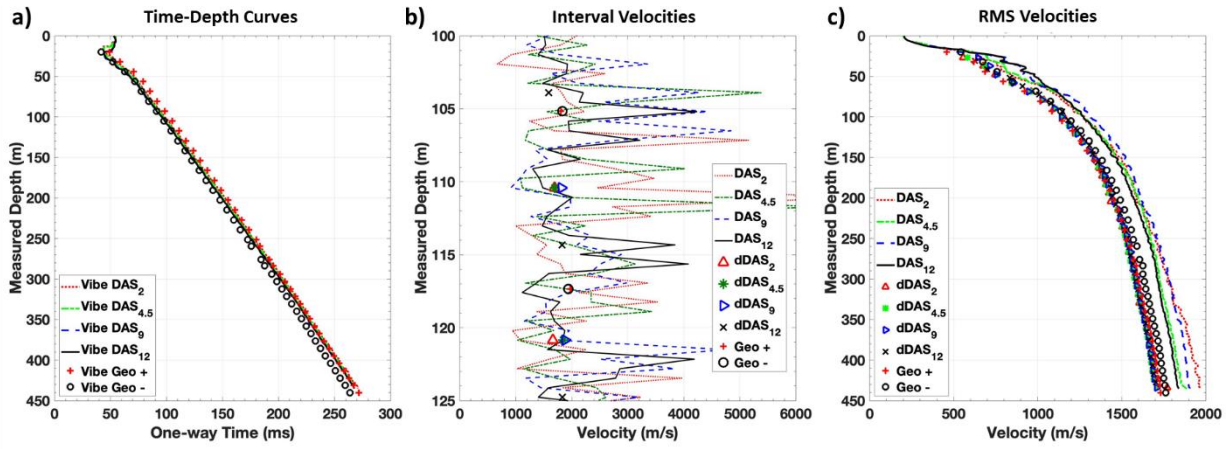

Figure 6: Traveltimes and velocities derived from the data: (a) time-depth curves obtained from the first-break picks for geophone and DAS data with various G_L; (b) Interval and (c) RMS velocities shown for different G_L and FBP decimation.

REFERENCES

Dean, T., T. Cuny, and A. Hartog, 2016, The effect of gauge length on axially incident P-waves measured using fibre optic distributed vibration sensing: Geophysical Prospecting, **65**, 184–193, doi: https://doi.org/10.1111/1365-2478.12419.

Hardeman-Vooys, H. K., and M. P. Lamoureux, 2019, Analytic models of distributed acoustic sensing data for straight and helical fibre: GeoConvention, 1–4.

Lizarralde, D., and S. Swift, 1999, Smooth inversion of VSP traveltime data: Geophysics, **64**, 659–661, doi: https://doi.org/10.1190/1.1444574.

Mateeva, A., J. Mestayer, B. Cox, D. Kiyashchenko, P. Wills, J. Lopez, S. Grandi, K. Hornman, P. Lumens, A. Franzen, D. Hill, and J. Roy, 2012, Advances in distributed acoustic sensing (DAS) for VSP: 82nd Annual International Meeting, SEG, Expanded Abstracts, 1–5, doi: https://doi.org/10.1190/segam2012-0739.1.

Mestayer, J., B. Cox, P. Willis, D. Kiyashchenko, J. Lopez, M. Costello, S. Bourne, G. Ugueto, R. Lupton, G. Solano, D. Hill, and A. Lewis, 2011, Field trials of distributed acoustic sensing for geophysical monitoring: 81st Annual International Meeting, SEG, Expanded Abstracts, 4253–4257, doi: https://doi.org/10.1190/1.3628095.

Willis, M., D. Barfoot, A. Ellmauthaler, X. Wu, O. Barrios, C. Erdemir, S. Shaw, and D. Quinn, 2016, Quantitative quality of distributed acoustic sensing vertical seismic profile data: The Leading Edge, **35**, 605–609, doi: https://doi.org/10.1190/tle35070605.1.

Wu, X., M. E. Willis, W. Palacios, A. Ellmauthaler, O. Barrios, S. Shaw, and D. Quinn, 2017, Compressional- and shear-wave studies of distributed acoustic sensing acquired vertical seismic profile data: The Leading Edge, **36**, 987–993, doi: https://doi.org/10.1190/tle36120987.1.